



Uniaxial deformation of nanowires in 16 refractory multi-principal element alloys



Shuzhi Xu ^a, Abdullah Al Mamun ^b, Sai Mu ^c, Yanqing Su ^{b,*}

^a School of Aerospace and Mechanical Engineering, University of Oklahoma, Norman, OK 73019-1052, USA

^b Department of Mechanical and Aerospace Engineering, Utah State University, Logan, UT 84322-4130, USA

^c Department of Physics and Astronomy, University of South Carolina, Columbia, SC 29208, USA

ARTICLE INFO

Article history:

Received 9 April 2023

Received in revised form 10 May 2023

Accepted 11 May 2023

Available online 19 May 2023

Keywords:

Metallic nanowire
Refractory multi-principal element alloys
Uniaxial deformation
Dislocation slip
Deformation twinning

ABSTRACT

Metallic nanowires are widely employed as small-scale structural materials due to their characteristically small volume and high strength compared with their bulk counterparts. Nowadays, the mechanical properties of nanowires in pure metals are well understood with the help of experiments and simulations. However, the deformation of nanowires in metallic alloys remains elusive. In recent years, a new class of alloys called refractory multi-principal element alloys (RMPEAs) emerged. RMPEAs are alloys that form solid solution phases and consist of three or more principal elements, most of which are refractory metals. In this paper, we perform atomistic simulations to investigate the uniaxial deformation of nanowires in 16 body-centered cubic RMPEAs. For each RMPEA, three nanowires consisting of atoms randomly distributed in three different ways are used. The main finding is that dislocation slips on {110} planes and twinning on {112} planes, respectively, control the compressive and tensile plastic deformation of the nanowires. To provide references, we also study the deformation of nanowires in natural and A-atom potential-based artificial pure metals. Results show that the deformation of RMPEA nanowires cannot be predicted by simply extrapolating from those of pure metal nanowires, highlighting the significance of directly simulating RMPEAs using multiple random atomic structures. It is also found that RMPEAs possess a reduced tension-compression asymmetry compared with pure metals, regardless of the underlying plastic deformation mechanism.

© 2023 Elsevier B.V. All rights reserved.

1. Introduction

Multi-principal element alloys (MPEAs) are a relatively new type of material consisting of multiple metallic elements in equal or nearly equal atomic fractions [1,2]. MPEAs are characterized by their complex chemistry since the number of possible equal-molar MPEAs increases exponentially with the number of principal elements [3]. The design space of non-equal-molar MPEAs is essentially boundless because the molar ratios among different elements can vary continuously [4]. Therefore, to obtain a deep understanding of MPEAs, it is critical to study their chemical compositions and structures at the atomic scale [5,6].

One popular modeling technique at the atomic scale is the atomistic simulation method. It has been applied to quasi-static deformation of bulk face-centered cubic (FCC) MPEAs, including, but not limited to, tension of Al_xCoCrCuFeNi [7], Al_{7.5}Co₂₅Cu_{17.5}Fe₂₅Ni₂₅ [8,9], CoCrCuFeNi [10–13,14], CoCrFeNi [15], CoCrFeNi(Al_{0.3}Ti_{0.2})_x (x = 0.25, 0.5, 0.75, or 1) [16], CoCrFeMnNi [17], non-equal-molar

CoCrFeMnNi and several subset ternaries and quaternaries [18], Co_xCr_yNi_{1-x-y} (0.2 ≤ x ≤ 0.6, 0.2 ≤ y ≤ 0.6) [19], and CoCuFeNiPd [20], shear of CoCrCuFeNi [14] and CoCrFeNi [21], as well as uniaxial deformation of Al_xCoCrFeNi [22–24], Al_xCoCu_{1-x}FeNi (x ≤ 0.4) [25,26], AlCrCuFeNi [27], AlCrCuFeNi_{1.4} [28], CoCrFeMnNi [29–32,33,34], and CoCrNi [35–38,39]. Fewer studies were devoted to bulk body-centered cubic (BCC) MPEAs, e.g., tension of HfNbTaZr [40] and non-equal-molar MoTiVZr [41], compression of AlCoCrCu_{0.5}Ni [42], Al_xCoCu_{1-x}FeNi (x > 0.4) [25], and MoNbTaW [43], shear of HfMoNbTaTi and HfNbTaTiZr [44], as well as uniaxial deformation of Al_xCrCoCuFeNi (x = 0.5 or 1.5) [45,46] and MoTaTiWZr [47,48]. These prior work investigated the effects of chemical composition, chemical short-range order, lamellae thickness, grain size, grain heterogeneity, crystallographic orientation, temperature, and strain rate on material properties, deformation mechanism, and mechanical properties such as elastic moduli, strength, and ductility.

Atomistic simulations were also applied to non-bulk MPEAs. The first class is 2D nanoplates, e.g., tension of FCC CoCrNi [49], non-equal-molar FCC CoCrNiFe [50], and BCC Al₃CoCrCuFeNi [51]. The second class is 1D nanowires, e.g., compression of BCC

* Corresponding author.

E-mail address: yanqing.su@usu.edu (Y. Su).

AlCoCrCu_{0.5}FeNi [52], BCC AlCoCrFeNi [53], and BCC AlMoWTa [54], as well as uniaxial deformation of FCC CoCrCuFeNi [55,56], FCC CoCrFeMn [57], and FCC CoCrFeMnNi [56,58–60]. The last class is 0D nanoparticles, e.g., tension of FCC CoCrFeMnNi [33,61] and compression of FCC Al_{0.25}CoCuFeNi_{0.75} and its subset ternaries and quaternaries [62]. Similar to bulk MPEAs, these studies involve influences of chemical composition, crystallographic orientation, temperature, and strain rate on mechanical responses.

One special type of BCC MPEAs is refractory MPEAs (RMPEAs) [63]. They consist of all or mostly refractory metals and can retain high strength at elevated temperatures, e.g., about half the melting point [64]. To date, deformation of RMPEAs has been explored via atomistic simulations only in bulk MoNbTaW [43], bulk HfMoNbTaTi, bulk HfNbTaTiZr [44], bulk HfNbTaZr [40], bulk MoTaTiWZr [47,48], bulk MoTiVZr [41], and AlMoWTa nanowire [54]. The last study revealed that its dominant deformation mechanism under compression is twinning produced by partial dislocations that are nucleated from the nanowire surface. In the meantime, other mechanisms such as slips of full dislocations and phase transformation were found to control plastic deformation in pure refractory BCC metallic nanowires such as those in Mo [65,66], Ta [65], V [67], and W [68–71,72,73]. Therefore, it is interesting to investigate deformation mechanisms in RMPEAs that are composed of these BCC metals.

Table 1
The 16 RMPEAs studied in this paper.

Ten ternaries	Five quaternaries	One quinary
MoNbTa, MoNbV, MoNbW, MoTaV, MoTaW, MoVW, NbTaV, NbTaW, NbVW, TaVW	MoNbTaV, MoNbTaW, MoNbVW, MoTaVW, NbTaVW	MoNbTaVW

In this paper, we explore uniaxial deformation, including tension and compression, of nanowires in 16 RMPEAs that are based on all five non-magnetic BCC refractory metals [74]: Mo, Nb, Ta, V, and W. These RMPEAs include ten ternaries, five quaternaries, and one quinary. Nanowires in the five constituent natural pure metals and 16 artificial pure metals enabled by A-atom potentials are also studied as references.

2. Materials and methods

2.1. Interatomic potentials

Embedded-atom method (EAM) potentials [75] are used to describe interatomic interactions. The five elemental potentials are: Mo [76], Nb [77], Ta [76], V [78], W [76]. These five BCC pure metals can form up to 16 equal-molar RMPEAs, as summarized in Table 1. Cross interactions among different elements are based on formulations of Johnson [79] and Zhou et al. [80]. In what follows, this type of interatomic potential is called “alloy potential”. Based on each alloy potential, an “A-atom potential” can be constructed to provide a mean-field representation of the RMPEA by approximating the interactions among different elements as a weighted average [81]. All alloy and A-atom potentials were recently developed by Xu et al. [82].

2.2. Atomistic simulations

First, simulation cells illustrated in Fig. 1 are constructed. The crystallographic orientations along the x, y, and z axes are [100], [010], and [001], respectively. In each cell, periodic boundary conditions are applied along the z axis while the boundaries along the x and y axes are traction-free, resulting in a nanowire with a circular cross-section. For each of the 16 RMPEAs, three random distributions of elements are used to form three nanowires. Each wire contains 1,429,014 atoms,

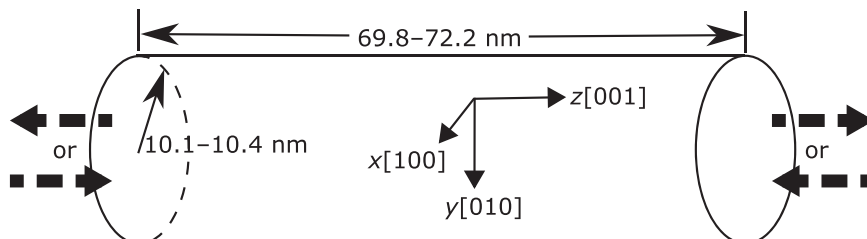


Fig. 1. Simulation cell of a nanowire. The uniaxial loading is applied along the z axis.

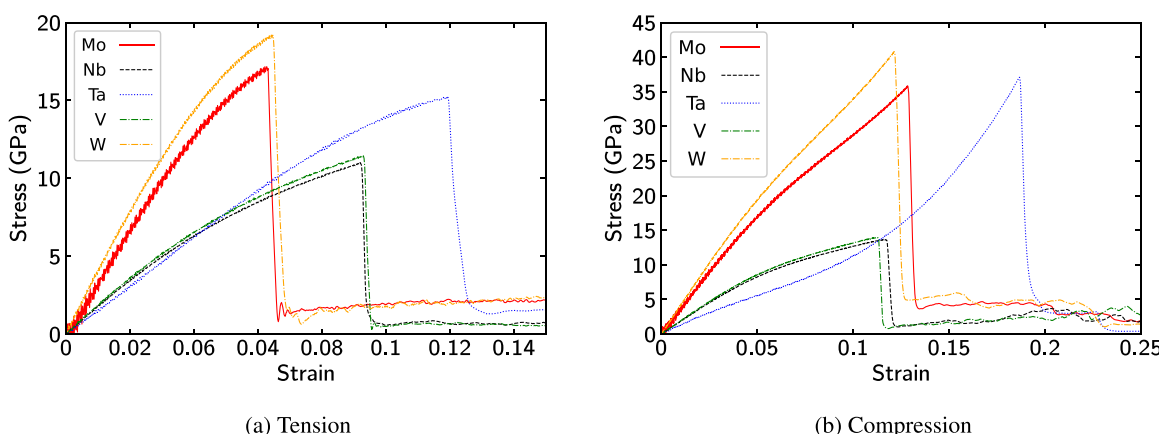


Fig. 2. Stress-strain curves based on (a) tension and (b) compression of nanowires in five constituent natural pure metals.

Table 2

Dominant plastic deformation mechanisms in nanowires in five constituent pure metals. DS: full dislocation slip; TW: twinning; PT: phase transformation.

	Mo	Nb	Ta	V	W
Tension	PT → TW	TW	TW	TW	PT → TW
Compression	DS	DS	DS	DS	DS

with its height being 69.8–72.2 nm and its radius 10.1–10.4 nm, depending on the lattice parameter of each RMPEA [82]. The length-to-radius aspect ratio is about 7, which is small enough to avoid buckling of the nanowire subject to compressive loading [69–71].

Second, atomistic simulations are performed using LAMMPS [83]. A velocity Verlet algorithm with a time step of 2 fs is employed to

update the atomic positions. Each cell is dynamically relaxed for 10,000 steps under isobaric zero stresses at 10 K. It follows that the conjugate gradient method is performed to minimize the system energy while zeroing the normal stress along the z axis. Then, at 10 K, a constant engineering strain rate $\dot{\epsilon} = \pm 10^8 \text{ s}^{-1}$ is applied along the z direction until the engineering strain reaches ± 0.25 . The effects of the strain rate were studied in a previous atomistic simulation work in W [70], where the stress-strain responses were found to converge once $|\dot{\epsilon}| \leq 10^8 \text{ s}^{-1}$.

The uniaxial engineering stress is calculated following the virial stress formulation. For reference, nanowires in the five constituent natural pure metals and 16 artificial pure metals enabled by A-atom potentials are also studied. Only one nanowire is used for each pure metal.

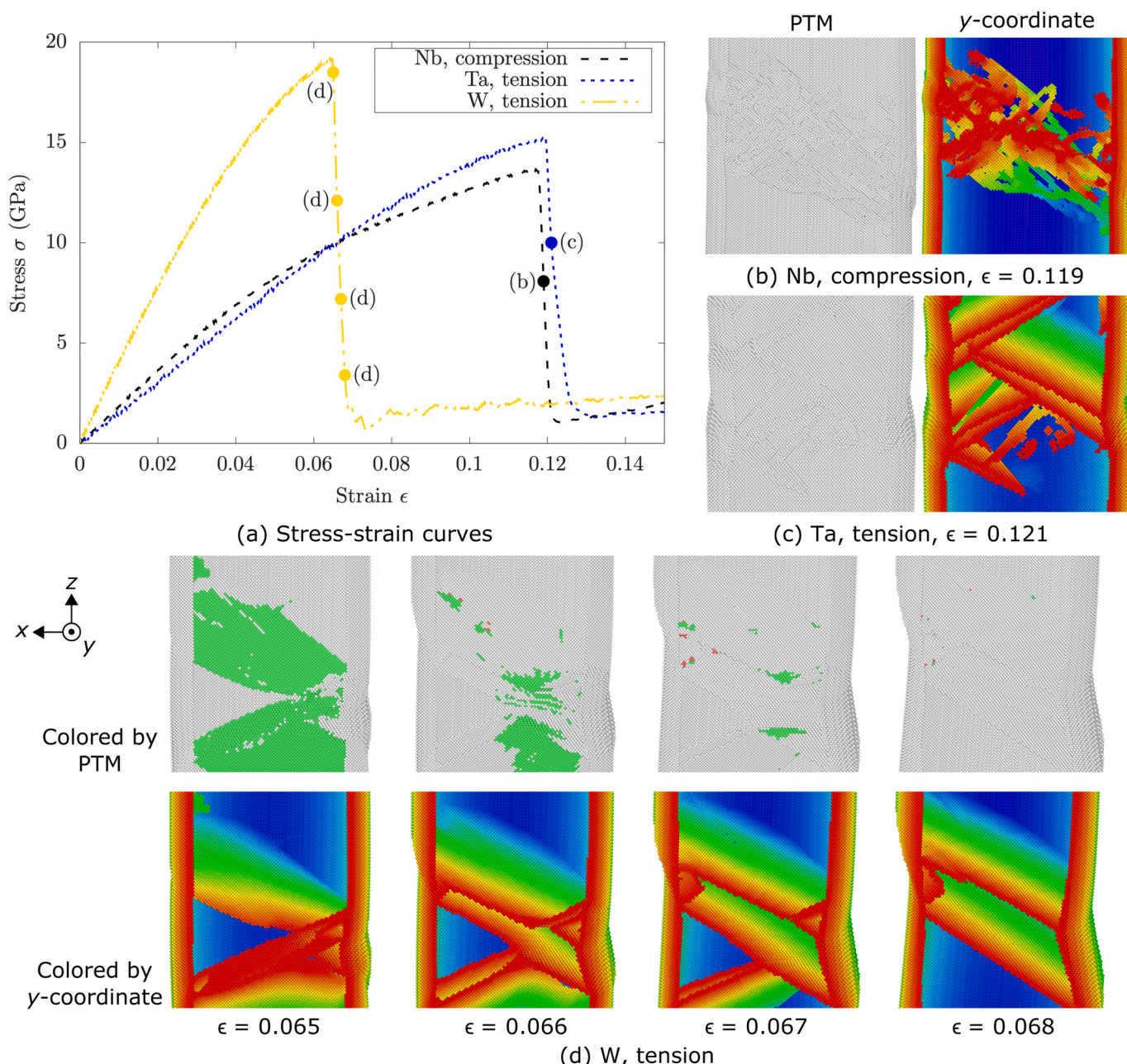


Fig. 3. (a) Three selected stress-strain curves in constituent pure metals, copied from Fig. 2. The filled circles correspond to atomic structures in (b–d). (b–d) Atomic structures of the initial stages of plastic deformation of nanowires in Nb, Ta, and W. Atoms are colored by the PTM method (green: FCC atoms; white: atoms in disordered lattice) or the y-coordinate. BCC atoms are deleted to highlight the defects. In (b), most dislocations are on {110} planes. In (c,d), most twin boundaries are on {112} planes.

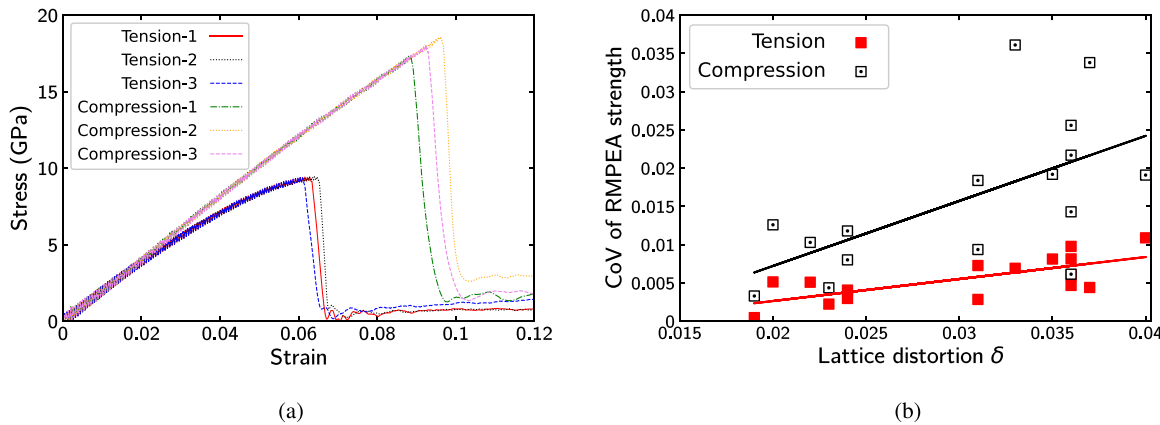


Fig. 4. (a) Six stress-strain curves for the quinary, MoNbTaVW, based on three different random atomic structures subject to either tensile or compressive loading. (b) CoV of the strengths of all 16 RMPEAs are plotted with respect to the lattice distortion. The dashed lines are linear fits for each type of loading.

In all cases, local atomic structures are classified by the polyhedral template matching (PTM) method [84] and atomic structures are visualized using OVITO [85].

2.3. Lattice distortion

The lattice distortion of each equal-molar RMPEA is characterized by [86].

$$\delta = \sqrt{\sum_{i=1}^n \frac{1}{n} \left(1 - \frac{a_i}{\sum_{i=1}^n a_i / n}\right)^2} \quad (1)$$

where n is the number of elements in the RMPEA and a_i is the lattice parameter of element i .

3. Results and discussions

3.1. Constituent natural pure metals: Mo, Nb, Ta, V, and W

Here, we present results of the five constituent natural pure metals: Mo, Nb, Ta, V, and W. Stress-strain responses based on tensile or compressive loading of nanowires in those five metals are given in Fig. 2. For the same metal, the compressive ultimate

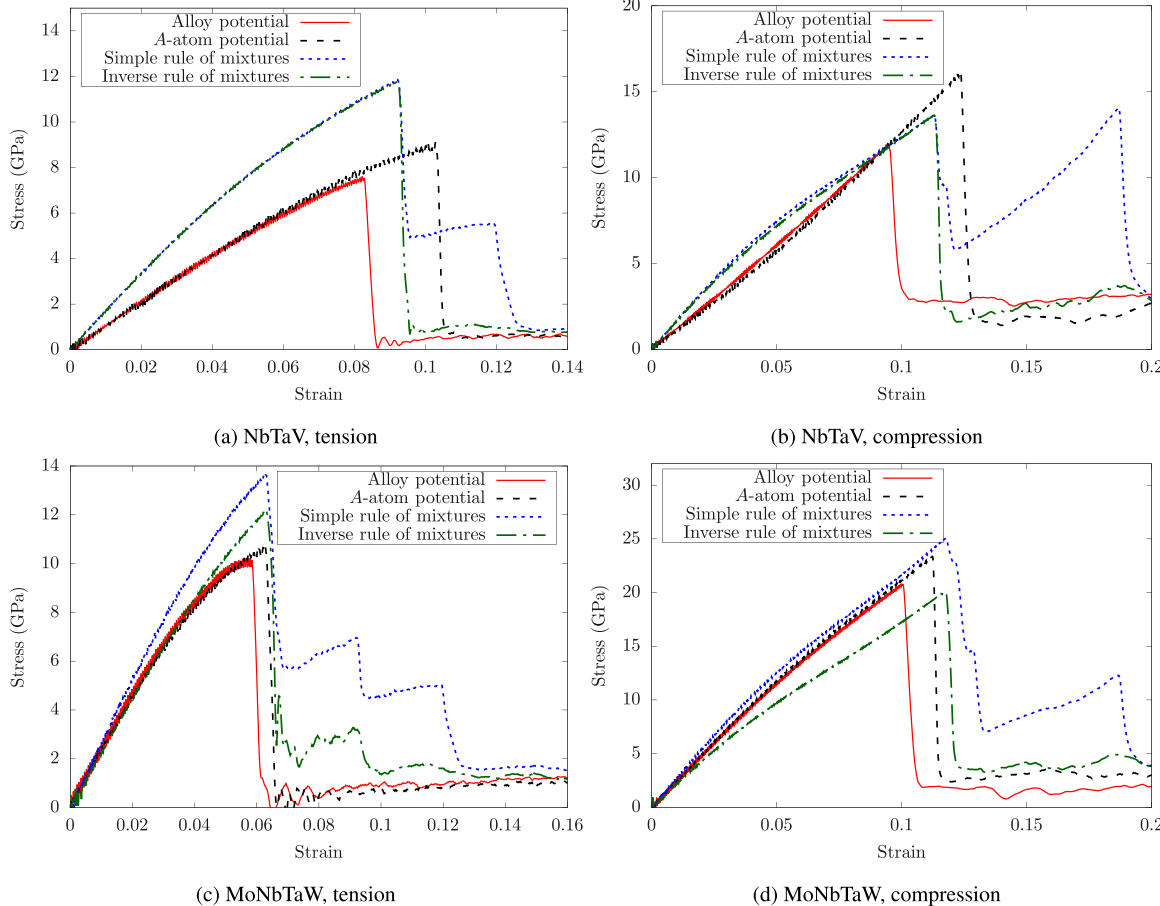


Fig. 5. Stress-strain curves of two selected RMPEA nanowires under tensile or compressive loading, obtained from four approaches.

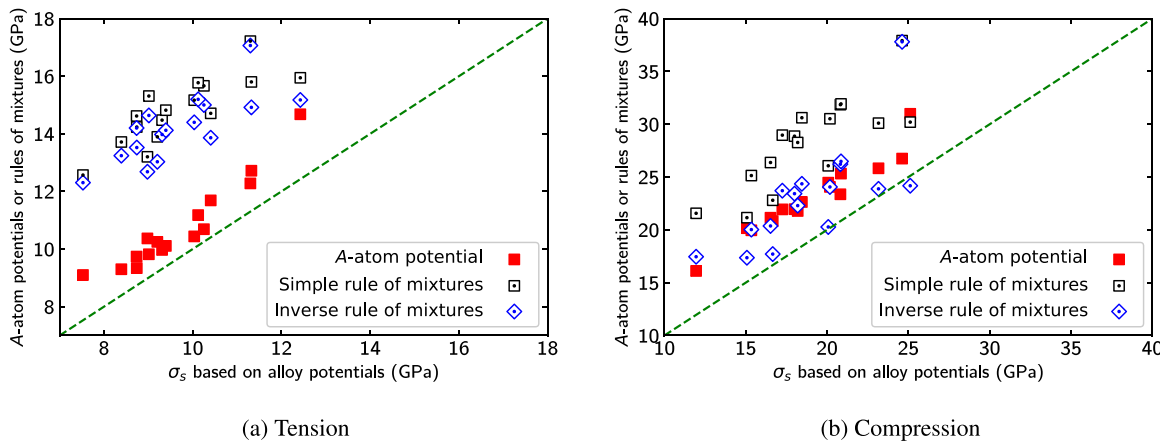


Fig. 6. Strengths of nanowires in 16 RMPEAs obtained from four approaches.

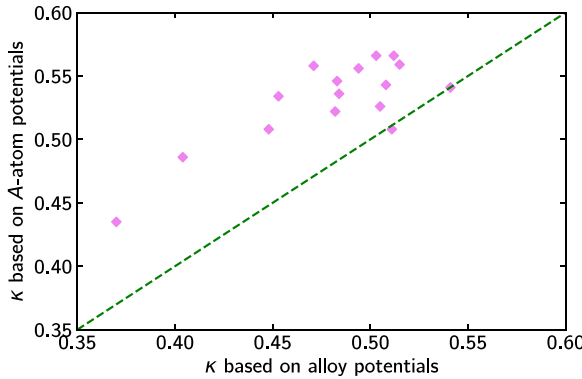


Fig. 7. Tension-compression asymmetry index κ for all 16 RMPEAs and 16 A-atom potential-based artificial pure metals.

strength more than doubles the tensile one in Mo, Ta, and W, while the former is only 22–24% higher than the latter in Nb and V. For both tensile and compressive loading, the ultimate strengths in the five metals are ranked as follows:

$$W > Mo \approx Ta > V \approx Nb \quad (2)$$

We now attempt to check whether the same trend had been reported in the literature, i.e., in other atomistic simulations of uniaxial deformation of dislocation-free single-crystalline nanowires in those five metals. To our best knowledge, there is no comparable prior study in Nb or Ta. So that leaves Mo [66], V [67], and W [68–70]. However, direct comparison is difficult because those simulations usually differ in temperature, strain rate, crystallographic orientation, and/or cross-sectional area size/shape. The two closest simulations are between Mo [66] and V [67]. In both cases, a tensile deformation was applied, the crystallographic orientation along the nanowire was $\langle 100 \rangle$, and the temperature was 300 K. However, they differed in two ways: the nanowire in Mo had a square cross-section, deformed at a strain rate of 10^8 s^{-1} ; the nanowire in V had a circular cross-section, deformed at a rate of $2 \times 10^8 \text{ s}^{-1}$. A prior atomistic study in W nanowires found that, with everything else being the same, (i) the two strain rates yielded the same strength and (ii) when the cross-sectional width was 5 nm, the strength was 11% higher should the nanowire have a circular cross-section than if it has a square cross-section [70]. Therefore, adjusted by the differences in strain rate and cross-sectional shape, the nanowire in Mo would have a strength of 15 GPa and 12 GPa, respectively, for a circular cross-sectional diameter of 4 nm and 6 nm [66], while the nanowire in V, with a diameter of 5 nm, has a strength of 11 GPa [67]. This suggests that, assuming a diameter of 5 nm, the strength in Mo

would be 23% higher than that in V, in qualitative agreement with the current study: 50% higher when the nanowire's diameter is about 20 nm. Note that this agreement is reached despite the different interatomic potentials used for the same metal. The comparison shows that our results are aligned with those in the literature and highlights the significance of systematically studying the deformation of nanowires in different metals.

Next, we analyze the dominant plastic deformation mechanisms in the five constituent pure metals. Results are summarized in Table 2. In compressive loading, the plastic deformation in all five metals is initiated by nucleation of full dislocations at the nanowire surface and sustained by continuous dislocation slips. Most dislocations are on $\{110\}$ planes, while no FCC atoms are formed in the cell, as shown in Fig. 3(b). Our results are in agreement with prior atomistic simulations of $\langle 112 \rangle$ W nanowires under compression, where interactions between W atoms are described by two other interatomic potentials [69,70]. In tensile loading, the yielding corresponds to twin embryos formed at the nanowire surface followed by subsequent twinning in Nb, Ta, and V (Fig. 3(c)). Most twin boundaries are on $\{112\}$ planes, with no FCC atoms adjacent to the twins. In a prior work, twinning was found to be the dominant plastic deformation mechanism in tensile loading of a $\langle 100 \rangle$ V nanowire, based on a modified EAM potential [67]. In tensile loading of the two remaining metals, Mo and W, the plasticity starts by localized BCC-to-FCC phase transformation followed by twinning formed in the same regions (Fig. 3(d)). In the literature, when a $\langle 100 \rangle$ nanowire was under tension, “twin bands with some irregular FCC structures” were observed in W based on the same interatomic potential used here [68] while twinning was reported as the only plasticity mechanism without any FCC atoms appearing in Mo to which a different interatomic potential [87] is applied [66]. Here, in all metals under either tension or compression, the emergence of dislocation slips, twinning, or phase transformation corresponds to the maximum stress, i.e., the ultimate strength. Thus, the maximum stress is taken as the yield strength in this paper.

3.2. RMPEAs and artificial pure metals

Here, we present results of 16 RMPEAs and their A-atom counterparts. First, we focus on the RMPEAs, i.e., those based on the alloy potentials. As mentioned in Sec. 2.2, three random distributions of elements are used for each RMPEA. As a result, three stress-strain curves are obtained for each RMPEA subject to either tensile or compressive loading. As an example, the six stress-strain curves for the quinary, MoNbTaVW, are presented in Fig. 4(a). Three tensile and three compressive strengths are then obtained for each RMPEA. It follows that the mean and coefficient of variation (CoV) of the three

strengths are calculated for all RMPEAs. In the remainder of this paper, any alloy potential-based result of each RMPEA is the mean value, unless stated otherwise. In the meantime, all CoV are plotted with respect to the lattice distortion δ in Fig. 4(b). Two phenomena are worth mentioning. First, for the same RMPEA, the CoV of compressive strength is higher than that of tensile strength. It may be attributed to their different plastic deformation mechanisms, as will be discussed later. Second, for the same type of loading, the CoV of strength scales positively with δ . Similar correlations were uncovered between the CoV of the basic structural parameters and the lattice distortion among 42 RMPEAs [82], which included the 16 alloys studied in this paper. Taken together, those results suggest that it is important to consider multiple atomic structures for the

same RMPEA in calculating material properties, especially when the alloy possesses a large lattice distortion.

Stress-strain responses based on tensile or compressive loading of nanowires in two selected RMPEAs are given in Fig. 5. Four stress-strain curves obtained from four different approaches are presented in each case: mean value from three direct calculations using the alloy potential, a single direct calculation using the A-atom potential, and simple or inverse rule of mixtures based on the stress-strain curves of the constituent pure metals. To better compare strengths obtained from different approaches, all strengths in all RMPEAs are summarized in Fig. 6. For each RMPEA under a given type of loading, the alloy potential and the simple rule of mixtures lead to the lowest and highest strengths among the four approaches, except in one

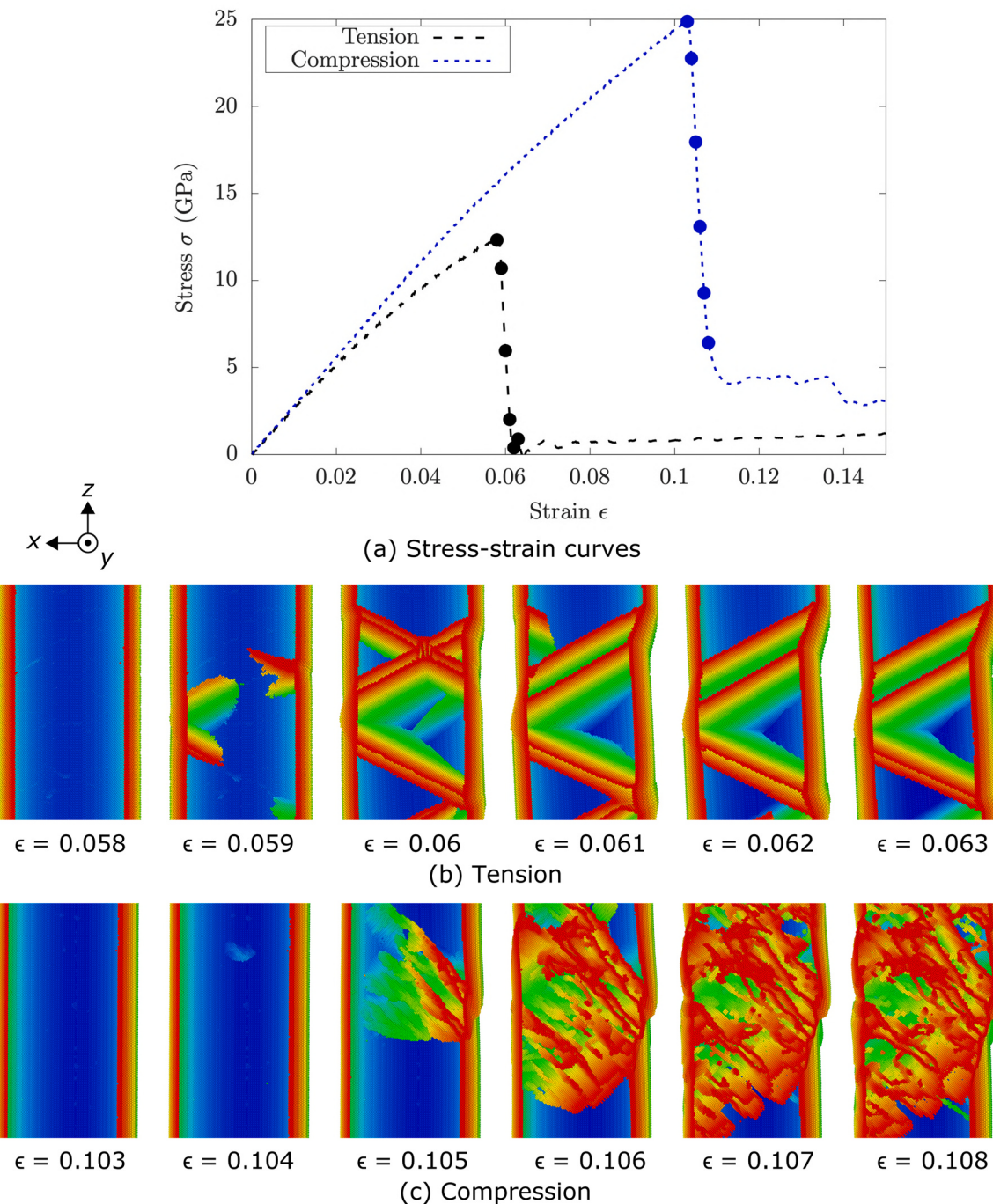


Fig. 8. (a) Two stress-strain curves in MoVW. The filled circles correspond to atomic structures in (b,c). In (b,c), atoms are colored by the y -coordinate. BCC atoms are deleted to highlight the defects. In (b), most twin boundaries are on {112} planes. In (c), most dislocations are on {110} planes.

case: compression of MoVW. In that special case, the A-atom potential and the inverse rule of mixtures predict the highest and lowest strengths, respectively. This exception may be due to that MoVW possesses the smallest lattice distortion, 0.019, among all RMPEAs studied here.

For the same type of stress-strain curve in the same RMPEA or its A-atom potential-based counterpart, the compressive strength is higher than the tensile strength, in agreement with that for natural pure metals. Here, we quantify the tension-compression asymmetry by an index κ , defined as

$$\kappa = \frac{\sigma_s^C - \sigma_s^T}{\sigma_s^C} \quad (3)$$

where the superscripts C and T denote compression and tension, respectively. κ can serve as a quantifier of the results of the tension-compression asymmetry, e.g., the Bauschinger effect. Values of κ for all 16 RMPEAs and their A-atom potential-based counterparts are plotted against each other in Fig. 7. Compared with their artificial pure metal counterparts, the tension-compression asymmetry is reduced in all alloys except MoNbW and MoTaW. This finding agrees with prior experiments [88] and simulations [89–91], where the dislocation was the only dominant plasticity carrier, that the plastic deformation becomes more homogeneous in RMPEAs than in pure metals. The current work additionally demonstrates that a reduced plastic anisotropy can be achieved in RMPEAs even when twinning controls the plastic deformation. For both dislocation slips and twinning, lattice distortion is considered the root cause of the

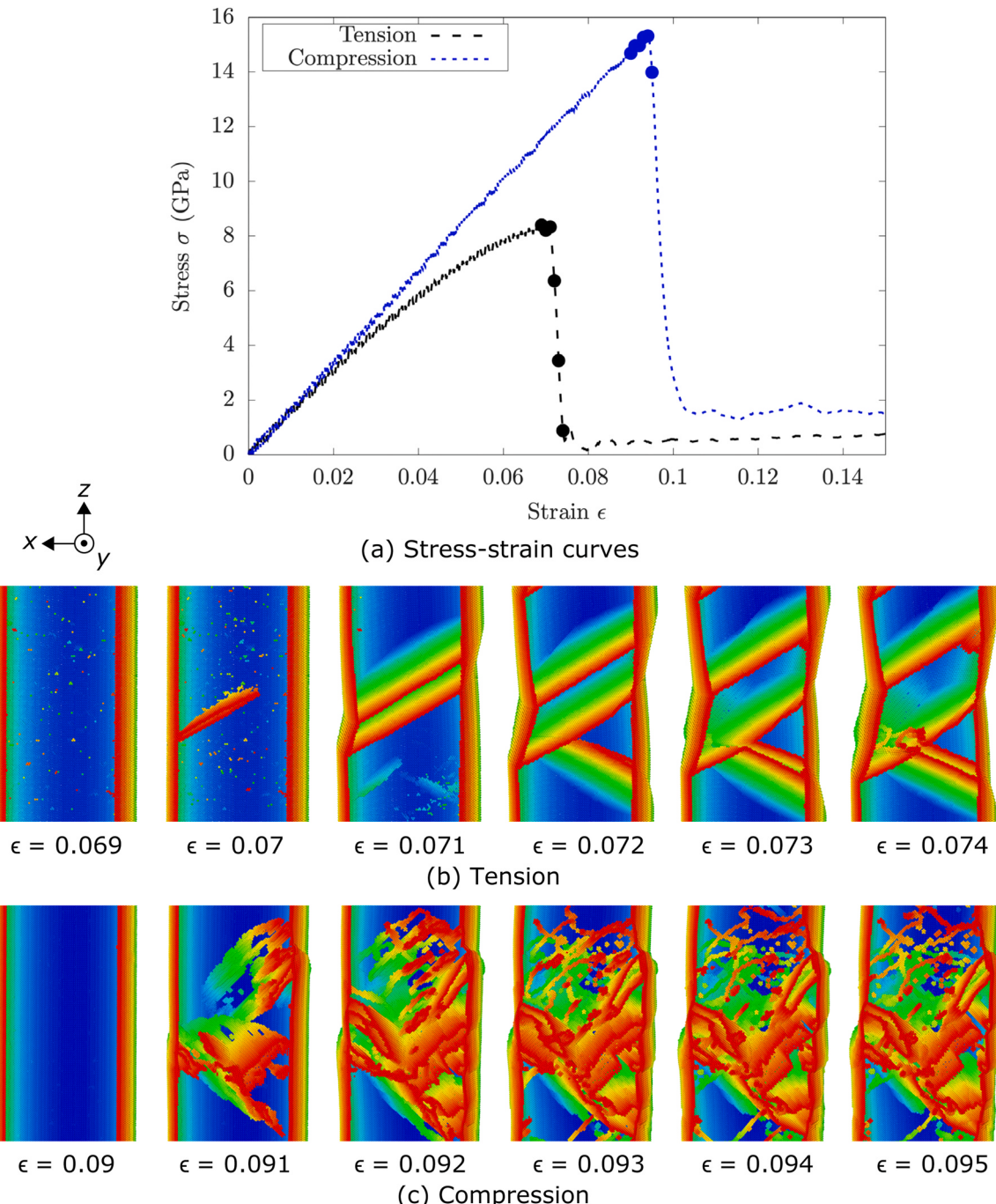


Fig. 9. Same as Fig. 8, but for MoNbTaV. In (b), some point-like defects exist when $0.069 \leq \epsilon \leq 0.071$.

homogeneous plasticity in MPEAs. In the meantime, unlike the plastic anisotropy, our recent work [82] showed that a RMPEA's elastic anisotropy is usually comparable with its constituent metals'. We note that a recent study found that the tension-compression asymmetry in plastic deformation increases with an increasing temperature in FCC AlCrCuFeNi [27].

The comparisons in Figs. 6 and 7 suggest that neither *A*-atom potential nor any rule of mixtures predicts the RMPEA strength well, although the former fares better. The main reason is that these approximations do not naturally capture the lattice distortion that is intrinsic to MPEAs. For example, the nanowire would have a rougher surface if it were modeled by an alloy potential than an *A*-atom potential. Prior atomistic simulations confirmed that nanowires with a rough surface have a lower yield strength than those with a

smooth one [92,93]. Thus, *A*-atom potentials result in higher yield strengths of nanowires than alloy potentials. Previous atomistic calculations in RMPEAs also showed that those approximations did not lead to accurate values of elastic constants [82,94], stacking fault energies [44,90,94], shear strengths [44,89,90], or local slip resistances [89,90]. Therefore, any property of a RMPEA predicted by the *A*-atom potential or any rule of mixtures, especially the latter, should be taken with caution.

Next, we analyze the dominant plastic deformation mechanisms in the 16 RMPEAs and their *A*-atom potential-based counterparts. Results in all those materials are uniform: twinning and dislocation slip, respectively, controls the plastic deformation of a nanowire under tension and compression. To demonstrate our simulation results, Figs. 8, 9, 10 present atomic structures at the initial stage of

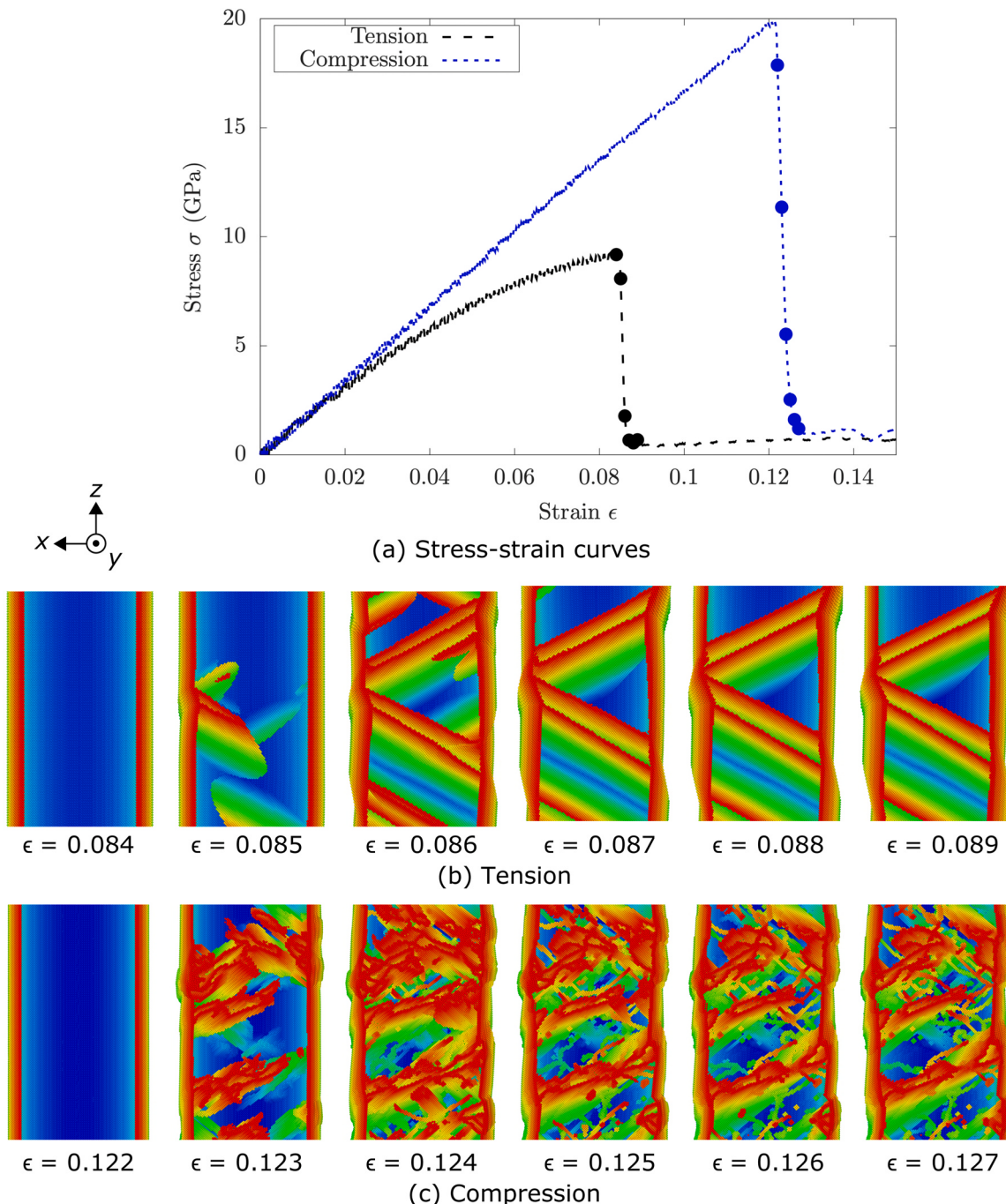


Fig. 10. Same as Figs. 8 and 9, but for an artificial pure metal based on the *A*-atom potential of MoNbTaV.

plasticity in two RMPEAs, MoVW and MoNbTaV, which have the smallest (0.019) and largest (0.037) lattice distortion, respectively, and an artificial pure metal based on the *A*-atom potential of MoNbTaV. As in natural pure metals, most dislocations are on {110} planes while most twin boundaries are on {112} planes.

Interestingly, right before the twin embryos are nucleated at the nanowire surface during the tensile loading of MoNbTaV, some point-like defects emerge. No such defects are found in either MoVW or *A*-atom potential-based MoNbTaV, suggesting that those defects are due to large lattice distortion. Another finding is that in none of RMPEAs or artificial pure metals were any FCC atoms identified at the initial stage of plastic deformation, unlike those in Mo and W nanowires under tension (Table 2). Again, this phenomenon suggests that the deformation mechanism of RMPEAs cannot be extrapolated simply from constituent pure metals.

It is interesting to compare the deformation mechanisms revealed in our atomistic simulations with those in the literature. However, our simulation temperature is low (10 K), and experiments of RMPEAs at cryogenic temperatures are rarely performed [95]. To our best knowledge, the only RMPEA that has been mechanically tested at cryogenic temperatures was HfNbTaTiZr. When it was subject to tension at 77 K, Wang et al. [96] reported dislocation slip on both {110} and {112} planes, deformation twinning on {112} planes, and BCC-to- ω phase transformation, while Eleti et al. [97] only observed dislocation slips on {112} planes. Although the experimental data are scarce and inconsistent, they suggest that dislocation slip, twinning, and phase transformation are all possible deformation mechanisms in RMPEAs at cryogenic temperatures.

4. Conclusions

In this work, atomistic simulations are conducted to explore the uniaxial deformation of nanowires in 16 RMPEAs, including ten ternaries, five quaternaries, and one quinary. These are all possible RMPEAs formed from the five non-magnetic BCC refractory pure metals: Mo, Nb, Ta, V, and W. As references, the nanowires in five constituent pure metals and 16 *A*-atom potential-based artificial pure metals are also studied. Main findings are summarized as follows:

1. Among the five constituent pure metals, for the same type of loading, W has the highest strength, followed by Mo and Ta, then with V and Nb possessing the lowest strengths. In compressive loading, dislocation slips on {110} planes are the main plastic deformation mechanism in all five metals. In tensile loading, {112} twinning controls the plasticity in all metals, except in Mo and W where the initial stage of twinning is accompanied by BCC-to-FCC phase transformation.
2. For each RMPEA, three stress-strain curves, and so three strengths, are obtained based on three different random atomic structures in the nanowire. Among all 16 RMPEAs, the CoV of strength scales positively with the lattice distortion, suggesting that it is important to consider multiple atomic structures in calculating the strengths, especially when the alloy possesses a large lattice distortion.
3. Among all 16 RMPEAs, four approaches are employed to predict the nanowire strengths: multiple direct calculations using the alloy potential, a single direct calculation using the *A*-atom potential, and simple or inverse rule of mixtures. Taking the first approach as the “right” one, the other three approaches do not predict the strength well. Using alloy and *A*-atom potentials, it is found that compressive and tensile plastic deformation, respectively, is controlled by dislocation slips on {110} planes and twinning on {112} planes. Correspondingly, for the alloy potentials, the CoV in compressive strength is higher than that in tensile strength.

4. In all RMPEAs and pure metals, the compressive strength is always higher than the tensile one. The tension-compression asymmetry is reduced in RMPEAs compared with pure metals, indicating a more homogeneous plastic deformation of the RMPEAs should they be subject to complex stress states.

CRediT authorship contribution statement

Shuozi Xu: Conceptualization, Methodology, Software, Formal analysis, Investigation, Data curation, Visualization, Writing – original draft, Writing – review & editing, Funding acquisition. **Abdullah Al Mamun:** Visualization. **Sai Mu:** Validation, Writing – review & editing. **Yanqing Su:** Conceptualization, Writing – original draft, Writing – review & editing, Supervision, Funding acquisition.

Data availability

Data will be made available on request.

Declaration of Competing Interest

The authors declare that they have no known competing financial interests or personal relationships that could have appeared to influence the work reported in this paper.

Acknowledgments

We thank Mr. Caleb Lounsbury for conducting simulations in pure refractory metals. This work used Bridges-2 at the Pittsburgh Supercomputing Center through allocation MAT220034 from the Advanced Cyberinfrastructure Coordination Ecosystem: Services & Support (ACCESS) program, which is supported by National Science Foundation grants #2138259, #2138286, #2138307, #2137603, and #2138296. The support and resources from the Center for High Performance Computing at the University of Utah are gratefully acknowledged. Some of the computing for this project was performed at the OU Supercomputing Center for Education & Research (OSCR) at the University of Oklahoma (OU). AAM and YS thank the start-up funds provided by the Utah State University.

References

- [1] J.-W. Yeh, S.-K. Chen, S.-J. Lin, J.-Y. Gan, T.-S. Chin, T.-T. Shun, C.-H. Tsau, S.-Y. Chang, Nanostructured high-entropy alloys with multiple principal elements: Novel alloy design concepts and outcomes, *Adv. Eng. Mater.* 6 (2004) 299–303, <https://doi.org/10.1002/adem.200300567>
- [2] B. Cantor, I.T.H. Chang, P. Knight, A.J.B. Vincent, Microstructural development in equiatomic multicomponent alloys, *Mater. Sci. Eng. A* 375–377 (2004) 213–218, <https://doi.org/10.1016/j.msea.2003.10.257>
- [3] Y.F. Ye, Q. Wang, J. Lu, C.T. Liu, Y. Yang, High-entropy alloy: challenges and prospects, *Mater. Today* 19 (2016) 349–362, <https://doi.org/10.1016/j.mattod.2015.11.026>
- [4] E.P. George, D. Raabe, R.O. Ritchie, High-entropy alloys, *Nat. Rev. Mater.* 4 (2019) 515–534, <https://doi.org/10.1038/s41578-019-0121-4>
- [5] Q. Jia, W. He, D. Hua, Q. Zhou, Y. Du, Y. Ren, Z. Lu, H. Wang, F. Zhou, J. Wang, Effects of structure relaxation and surface oxidation on nanoscopic wear behaviors of metallic glass, *Acta Mater.* 232 (2022) 117934, <https://doi.org/10.1016/j.actamat.2022.117934>
- [6] Y. Ren, T. Yan, Z. Huang, Q. Zhou, K. Hua, X. Li, Y. Du, Q. Jia, L. Zhang, H. Zhang, H. Wang, Cryogenic wear behaviors of a metastable Ti-based bulk metallic glass composite, *J. Mater. Sci. Technol.* 134 (2023) 33–41, <https://doi.org/10.1016/j.jmst.2022.06.027>
- [7] J. Li, H. Chen, S. Li, Q. Fang, Y. Liu, L. Liang, H. Wu, P.K. Liaw, Tuning the mechanical behavior of high-entropy alloys via controlling cooling rates, *Mater. Sci. Eng. A* 760 (2019) 359–365, <https://doi.org/10.1016/j.msea.2019.06.017>
- [8] J. Li, Q. Fang, B. Liu, Y. Liu, Transformation induced softening and plasticity in high entropy alloys, *Acta Mater.* 147 (2018) 35–41, <https://doi.org/10.1016/j.actamat.2018.01.002>
- [9] L. Li, H. Chen, Q. Fang, J. Li, F. Liu, Y. Liu, P.K. Liaw, Effects of temperature and strain rate on plastic deformation mechanisms of nanocrystalline high-entropy alloys, *Intermetallics* 120 (2020) 106741, <https://doi.org/10.1016/j.intermet.2020.106741>

- [10] J. Liu, Molecular dynamic study of temperature dependence of mechanical properties and plastic inception of CoCrCuFeNi high-entropy alloy, Phys. Lett. A 384 (2020) 126516, , <https://doi.org/10.1016/j.physleta.2020.126516>
- [11] L. Zhang, Y. Shibuta, Inverse Hall-Petch relationship of high-entropy alloy by atomistic simulation, Mater. Lett. 274 (2020) 128024, , <https://doi.org/10.1016/j.matlet.2020.128024>
- [12] D. Farkas, Deformation behavior of a model high entropy alloy from atomistic simulations, Mater. Sci. Eng. A 812 (2021) 141124, , <https://doi.org/10.1016/j.msea.2021.141124>
- [13] O.R. Deluigi, F. Valencia, N. Amigo, F. Aquistapace, R.I. Gonzalez, E.M. Bringa, Atomistic simulations of tensile deformation of a nanoporous high-entropy alloy, J. Mater. Sci. 57 (2022) 19817–19831, <https://doi.org/10.1007/s10853-022-07862-w>
- [14] A.M. Kazakov, A.V. Yakhin, E.Z. Karimov, R.I. Babicheva, A.A. Kistanov, E.A. Korznikova, Effect of segregation on deformation behaviour of nanoscale CoCrFeNi high-entropy alloy, Appl. Sci. 13 (2023) 4013, <https://doi.org/10.3390/app13064013>
- [15] L. Li, B. Xie, Q. Fang, J. Li, Machine learning approach to design high entropy alloys with heterogeneous grain structures, Metall. Mater. Trans. A 52 (2021) 439–448, <https://doi.org/10.1007/s11661-020-06099-z>
- [16] Z.H. Sun, J. Zhang, G.X. Xin, L. Xie, L.C. Yang, Q. Peng, Tensile mechanical properties of CoCrFeNiTiAl high entropy alloy via molecular dynamics simulations, Intermatallics 142 (2022) 107444, , <https://doi.org/10.1016/j.intermet.2021.107444>
- [17] J. Li, B. Xie, Q. He, B. Liu, X. Zeng, P.K. Liaw, Q. Fang, Y. Yang, Y. Liu, Chemical-element-distribution-mediated deformation partitioning and its control mechanical behavior in high-entropy alloys, J. Mater. Sci. Technol. 120 (2022) 99–107, <https://doi.org/10.1016/j.jmst.2021.11.065>
- [18] S.K. Singh, A. Parashar, Defect dynamics and uniaxial tensile deformation of equi and non-equi-atomic configuration of multi-elemental alloys, Mater. Chem. Phys. 266 (2021) 124549, , <https://doi.org/10.1016/j.matchemphys.2021.124549>
- [19] J. Li, B. Xie, Q. Fang, B. Liu, Y. Liu, P.K. Liaw, High-throughput simulation combined machine learning search for optimum elemental composition in medium entropy alloy, J. Mater. Sci. Technol. 68 (2021) 70–75, <https://doi.org/10.1016/j.jmst.2020.08.008>
- [20] S. Chen, Z.H. Aitken, S. Pattamatta, Z. Wu, Z.G. Yu, D.J. Srolovitz, P.K. Liaw, Y.-W. Zhang, Simultaneously enhancing the ultimate strength and ductility of high-entropy alloys via short-range ordering, Nat. Commun. 12 (2021) 4953, <https://doi.org/10.1038/s41467-021-25264-5>
- [21] R. Babicheva, A. Jarlöv, H. Zheng, S. Dmitriev, E. Korznikova, M. LingSharonNai, U. Ramamurtty, K. Zhou, Effect of short-range ordering and grain boundary segregation on shear deformation of CoCrFeNi high-entropy alloys with Al addition, Comput. Mater. Sci. 215 (2022) 111762, , <https://doi.org/10.1016/j.commatsci.2022.111762>
- [22] A. Sharma, P. Singh, D.D. Johnson, P.K. Liaw, G. Balasubramanian, Atomistic clustering-ordering and high-strain deformation of an $Al_{0.1}CrCoFeNi$ high-entropy alloy, Sci. Rep. 6 (2016) 31028, <https://doi.org/10.1038/srep31028>
- [23] A. Sharma, G. Balasubramanian, Dislocation dynamics in $Al_xCoCrFeNi$ high-entropy alloy under tensile loading, Intermatallics 91 (2017) 31–34, <https://doi.org/10.1016/j.intermet.2017.08.004>
- [24] J. Jiang, P. Chen, J. Qiu, W. Sun, I. Saikov, V. Shcherbakov, M. Alymov, Microstructural evolution and mechanical properties of $Al_xCoCrFeNi$ high-entropy alloys under uniaxial tension: a molecular dynamics simulations study, Mater. Today Comm. 28 (2021) 102525, , <https://doi.org/10.1016/j.mtcomm.2021.102525>
- [25] S. Chen, Z.H. Aitken, Z. Wu, Z. Yu, R. Banerjee, Y.-W. Zhang, Hall-Petch and inverse Hall-Petch relations in high-entropy $CoNiFeAl_{1-x}Cu_{1-x}$ alloys, Mater. Sci. Eng. A 773 (2020) 138873, , <https://doi.org/10.1016/j.msea.2019.138873>
- [26] L. Wang, W. Liu, B. Zhu, W. Chen, F. Zhang, B. Liu, J. Liu, J. Zhou, Y. Zhao, Influences of strain rate, Al concentration and grain heterogeneity on mechanical behavior of $CoNiFeAl_{1-x}$ high-entropy alloys: a molecular dynamics simulation, J. Mater. Res. Technol. 14 (2021) 2071–2084, <https://doi.org/10.1016/j.jmrt.2021.07.116>
- [27] H.-G. Nguyen, T.-H. Fang, D.-Q. Doan, Cyclic plasticity and deformation mechanism of $AlCrCuFeNi$ high entropy alloy, J. Alloy. Compd. 940 (2023) 168838, , <https://doi.org/10.1016/j.jallcom.2023.168838>
- [28] J. Li, Q. Fang, B. Liu, Y. Liu, Y. Liu, Mechanical behaviors of $AlCrFeCuNi$ high-entropy alloys under uniaxial tension via molecular dynamics simulation, RSC Adv. 6 (2016) 76409–76419, <https://doi.org/10.1039/C6RA16503F>
- [29] Y. Qi, X. Chen, M. Feng, Molecular dynamics-based analysis of the effect of temperature and strain rate on deformation of nanocrystalline $CoCrFeMnNi$ high-entropy alloy, Appl. Phys. A 126 (2020) 529, <https://doi.org/10.1007/s00339-020-03714-z>
- [30] Y. Qi, H. Xu, T. He, M. Wang, M. Feng, Atomistic simulation of deformation behaviors polycrystalline $CoCrFeMnNi$ high-entropy alloy under uniaxial loading, Int. J. Refract. Met. Hard Mater. 95 (2021) 105415, , <https://doi.org/10.1016/j.ijrmhm.2020.105415>
- [31] L. Zhang, K. Qian, J. Huang, M. Liu, Y. Shibuta, Molecular dynamics simulation and machine learning of mechanical response in non-equiautomic $FeCrNiCoMn$ high-entropy alloy, J. Mater. Res. Technol. 13 (2021) 2043–2054, <https://doi.org/10.1016/j.jmrt.2021.06.021>
- [32] J. Xiao, N. Wu, O. Ojo, C. Deng, Stacking fault and transformation-induced plasticity in nanocrystalline high-entropy alloys, J. Mater. Res. 36 (2021) 2705–2714, <https://doi.org/10.1557/s43578-021-00140-6>
- [33] K.-T. Chen, T.-J. Wei, G.-C. Li, M.-Y. Chen, Y.-S. Chen, S.-W. Chang, H.-W. Yen, C.-S. Chen, Mechanical properties and deformation mechanisms in $CoCrFeMnNi$ high entropy alloys: a molecular dynamics study, Mater. Chem. Phys. 271 (2021) 124912, , <https://doi.org/10.1016/j.matchemphys.2021.124912>
- [34] T. Guo, L. Wu, T. Li, Machine learning accelerated, high throughput, multi-objective optimization of multiprincipal element alloys, Small 17 (2021) 2102972, , <https://doi.org/10.1002/smll.202102972>
- [35] F. Yuan, W. Cheng, S. Zhang, X. Liu, X. Wu, Atomistic simulations of tensile deformation in a $CrCoNi$ medium-entropy alloy with heterogeneous grain structures, Materialia 9 (2020) 100565, , <https://doi.org/10.1016/j.mtla.2019.100565>
- [36] W.-R. Jian, Z. Xie, S. Xu, Y. Su, X. Yao, I.J. Beyerlein, Effects of lattice distortion and chemical short-range order on the mechanisms of deformation in medium entropy alloy $CoCrNi$, Acta Mater. 199 (2020) 352–369, <https://doi.org/10.1016/j.actamat.2020.08.044>
- [37] Y. Ma, M. Yang, F. Yuan, X. Wu, Deformation induced hcp nano-lamella and its size effect on the strengthening in a $CoCrNi$ medium-entropy alloy, J. Mater. Sci. Technol. 82 (2021) 122–134, <https://doi.org/10.1016/j.jmst.2020.12.017>
- [38] Z. Xie, W.-R. Jian, S. Xu, I.J. Beyerlein, X. Zhang, X. Yao, R. Zhang, Phase transition in medium entropy alloy $coCrNi$ under quasi-isentropic compression, Int. J. Plast. 157 (2022) 103389, , <https://doi.org/10.1016/j.ijplas.2022.103389>
- [39] A. Gupta, W.-R. Jian, S. Xu, I.J. Beyerlein, G.J. Tucker, On the deformation behavior of $coCrNi$ medium-entropy alloys: Unraveling mechanistic competition, Int. J. Plast. 158 (2022) 103442, , <https://doi.org/10.1016/j.ijplas.2022.103442>
- [40] F. Aquistapace, N. Vazquez, M. Chiarpotti, O. Deluigi, C.J. Ruestes, E.M. Bringa, Atomistic simulations of ductile failure in a b.c.c. high-entropy alloy, High. Entropy Alloy. Mater. (2022), <https://doi.org/10.1007/s44210-022-00004-6>
- [41] B. Chen, J. Sun, L. Zhuo, T. Yan, B. Sun, M. Zhan, An atomistic study of the newly-developed single-phase refractory high entropy alloy of $TiZrVMo$: Defect accumulation and evolution under tensile deformation, Mater. Lett. 333 (2023) 133664, , <https://doi.org/10.1016/j.matlett.2022.133664>
- [42] S. Feng, L. Li, K.C. Chan, L. Zhao, S. Pan, L. Wang, R. Liu, Tuning deformation behavior of $Cu_0.5CoNiCrAl$ high-entropy alloy via cooling rate gradient: An atomistic study, Intermatallics 112 (2019) 106553, , <https://doi.org/10.1016/j.intermet.2019.106553>
- [43] X.-G. Li, C. Chen, H. Zheng, Y. Zuo, S.P. Ong, Complex strengthening mechanisms in the $NbMoTaW$ multi-principal element alloy, npj Comput. Mater. 6 (2020) 70, <https://doi.org/10.1038/s41524-020-0339-0>
- [44] S. Xu, W.-R. Jian, I.J. Beyerlein, Ideal simple shear strengths of two $HfNbTaTi$ -based quinary refractory multi-principal element alloys, APL Mater. 10 (2022) 11107, , <https://doi.org/10.1063/5.0116898>
- [45] M. Bahramyan, R. TaherzadehMousavian, D. Brabazon, Determination of atomic-scale structure and compressive behavior of solidified $Al_xCrCoFeCuNi$ high entropy alloys, Int. J. Mech. Sci. 171 (2020) 105389, , <https://doi.org/10.1016/j.ijmecsci.2019.105389>
- [46] M. Bahramyan, R.T. Mousavian, D. Brabazon, Study of the plastic deformation mechanism of TRIP-TWIP high entropy alloys at the atomic level, Int. J. Plast. 127 (2020) 102649, , <https://doi.org/10.1016/j.ijplas.2019.102649>
- [47] P. Singh, A. Sharma, A.V. Smirnov, M.S. Diallo, P.K. Ray, G. Balasubramanian, D.D. Johnson, Design of high-strength refractory complex solid-solution alloys, npj Comput. Mater. 4 (2018) 16, <https://doi.org/10.1038/s41524-018-0072-0>
- [48] A. Sharma, P. Singh, T. Kirk, V.I. Levitas, P.K. Liaw, G. Balasubramanian, R. Arroyave, D.D. Johnson, Pseudoelastic deformation in Mo-based refractory multi-principal element alloys, Acta Mater. 220 (2021) 117299, , <https://doi.org/10.1016/j.actamat.2021.117299>
- [49] J. Li, L. Li, C. Jiang, Q. Fang, F. Liu, Y. Liu, P.K. Liaw, Probing deformation mechanisms of gradient nanostructured $CrCoNi$ medium entropy alloy, J. Mater. Sci. Technol. 57 (2020) 85–91, <https://doi.org/10.1016/j.jmst.2020.03.064>
- [50] A. Jarlöv, W. Ji, Z. Zhu, Y. Tian, R. Babicheva, R. An, H.L. Seet, M.L.S. Nai, K. Zhou, Molecular dynamics study on the strengthening mechanisms of Cr-Fe-Co-Ni high-entropy alloys based on the generalized stacking fault energy, J. Alloy. Compd. 905 (2022) 164137, , <https://doi.org/10.1016/j.jallcom.2022.164137>
- [51] J. Peng, L. Li, F. Li, B. Liu, S. Zherebtsov, Q. Fang, J. Li, N. Stepanov, Y. Liu, P.K. Liaw, The predicted rate-dependent deformation behaviour and multistage strain hardening in a model heterostructured body-centered cubic high entropy alloy, Int. J. Plast. 145 (2021) 103073, , <https://doi.org/10.1016/j.ijplas.2021.103073>
- [52] W. Li, J. Tang, Q. Wang, H. Fan, Molecular dynamics simulations on the mechanical behavior of $AlCoCrCu_{0.5}FeNi$ high-entropy alloy nanopillars, TMS 2019 148th Annual Meeting & Exhibition Supplemental Proceedings, The Minerals, Metals & Materials Series, Springer International Publishing, Cham, 2019, pp. 1271–1280, https://doi.org/10.1007/978-3-030-05861-6_121
- [53] Q. Zhang, R. Huang, X. Zhang, T. Cao, Y. Xue, X. Li, Deformation mechanisms and remarkable strain hardening in single-crystalline high-entropy-alloy micro-pillars/nanopillars, Nano Lett. 21 (2021) 3671–3679, <https://doi.org/10.1021/acs.nanolett.1c00444>
- [54] Z.H. Aitken, Y.-W. Zhang, Revealing the deformation twinning nucleation mechanism of BCC HEAs, MRS Commun. 9 (2019) 406–412, <https://doi.org/10.1557/mrc.2019.16>
- [55] C.J. Ruestes, D. Farkas, Deformation response of high entropy alloy nanowires, J. Mater. Sci. 56 (2021) 16447–16462, <https://doi.org/10.1007/s10853-021-06314-1>
- [56] Y. Cui, Y. Toku, Y. Ju, Nanotwinning and tensile behavior in cold-welded high-entropy-alloy nanowires, Nanotechnology 32 (2021) 315716, , <https://doi.org/10.1088/1361-6528/abf7eb>
- [57] P. Wang, Y. Lin, Y. Cao, H. Zhao, Q. Li, H. Wang, Atomistic simulations of martensitic transformation processes for metastable $FeMnCoCr$ high-entropy alloy, Sci. China Technol. Sci. 66 (2023) 998–1006, <https://doi.org/10.1007/s11431-022-2146-9>
- [58] J. Xiao, C. Deng, Martensite transformation induced superplasticity and strengthening in single crystalline $CoNiCrFeMn$ high entropy nanowires: a

- molecular dynamics study, *Mater. Sci. Eng. A* 793 (2020) 139853, , <https://doi.org/10.1016/j.msea.2020.139853>
- [59] P.K. Tripathi, Y.-C. Chiu, S. Bhowmick, Y.-C. Lo, Temperature-dependent superplasticity and strengthening in CoNiCrFeMn high entropy alloy nanowires using atomistic simulations, *Nanomaterials* 11 (2021) 2111, <https://doi.org/10.3390/nano11082111>
- [60] H.-F. Zhang, H.-L. Yan, F. Fang, N. Jia, Orientation-dependent mechanical responses and plastic deformation mechanisms of FeMnCoCrNi high-entropy alloy: a molecular dynamics study, *Acta Metall. Sin. Engl. Lett.* 34 (2021) 1511–1526, <https://doi.org/10.1007/s40195-021-01260-y>
- [61] W.-M. Choi, Y.H. Jo, S.S. Sohn, S. Lee, B.-J. Lee, Understanding the physical metallurgy of the CoCrFeMnNi high-entropy alloy: an atomistic simulation study, *npj Comput. Mater.* 4 (2018) 1, <https://doi.org/10.1038/s41524-017-0060-9>
- [62] W. Li, H. Fan, J. Tang, Q. Wang, X. Zhang, J.A. El-Awady, Effects of alloying on deformation twinning in high entropy alloys, *Mater. Sci. Eng. A* 763 (2019) 138143, , <https://doi.org/10.1016/j.msea.2019.138143>
- [63] O.N. Senkov, G.B. Wilks, D.B. Miracle, C.P. Chuang, P.K. Liaw, Refractory high-entropy alloys, *Intermetallics* 18 (2010) 1758–1765, <https://doi.org/10.1016/j.intermet.2010.05.014>
- [64] O.N. Senkov, S. Gorsse, D.B. Miracle, High temperature strength of refractory complex concentrated alloys, *Acta Mater.* 175 (2019) 394–405, <https://doi.org/10.1016/j.actamat.2019.06.032>
- [65] C.R. Weinberger, W. Cai, Surface-controlled dislocation multiplication in metal micropillars, *Proc. Natl. Acad. Sci. USA* 105 (2008) 14304–14307, <https://doi.org/10.1073/pnas.0806118105>
- [66] P. Wang, W. Chou, A. Nie, Y. Huang, H. Yao, H. Wang, Molecular dynamics simulation on deformation mechanisms in body-centered-cubic molybdenum nanowires, *J. Appl. Phys.* 110 (2011) 093521, , <https://doi.org/10.1063/1.3660251>
- [67] L. Wang, H. Deng, S. Xiao, W. Hu, Effect of voids on the tensile properties of vanadium nanowires, *Nucl. Instrum. Methods Phys. Res. B* 303 (2013) 14–17, <https://doi.org/10.1016/j.nimb.2013.03.023>
- [68] B. Ma, Q.-h. Rao, Y.-h. He, Effect of crystal orientation on tensile mechanical properties of single-crystal tungsten nanowire, *Trans. Nonferr. Met. Soc. China* 24 (2014) 2904–2910, [https://doi.org/10.1016/S1003-6326\(14\)63425-7](https://doi.org/10.1016/S1003-6326(14)63425-7)
- [69] S. Xu, J.K. Startt, T.G. Payne, C.S. Deo, D.L. McDowell, Size-dependent plastic deformation of twinned nanopillars in body-centered cubic tungsten, *J. Appl. Phys.* 121 (2017) 175101, , <https://doi.org/10.1063/1.4982754>
- [70] S. Xu, Y. Su, D. Chen, L. Li, An atomistic study of the deformation behavior of tungsten nanowires, *Appl. Phys. A* 123 (2017) 788, <https://doi.org/10.1007/s00339-017-1414-3>
- [71] S. Xu, S.Z. Chavoshi, Uniaxial deformation of nanotwinned nanotubes in body-centered cubic tungsten, *Curr. Appl. Phys.* 18 (2018) 114–121, <https://doi.org/10.1016/j.cap.2017.10.003>
- [72] S. Xu, S.Z. Chavoshi, Y. Su, Deformation mechanisms in nanotwinned tungsten nanopillars: Effects of coherent twin boundary spacing, *Phys. Stat. Solidi RRL* 12 (2018) 1700399, , <https://doi.org/10.1002/pssr.201700399>
- [73] T. Trusty, S. Xu, I.J. Beyerlein, Atomistic simulations of tungsten nanotubes under uniform tensile loading, *J. Appl. Phys.* 126 (2019) 095105, , <https://doi.org/10.1063/1.5110167>
- [74] S. Xu, Y. Su, L.T.W. Smith, I.J. Beyerlein, Frank-Read source operation in six body-centered cubic refractory metals, *J. Mech. Phys. Solids* 141 (2020) 104017, , <https://doi.org/10.1016/j.jmps.2020.104017>
- [75] M.S. Daw, M.I. Baskes, Embedded-atom method: Derivation and application to impurities, surfaces, and other defects in metals, *Phys. Rev. B* 29 (1984) 6443–6453, <https://doi.org/10.1103/PhysRevB.29.6443>
- [76] X.W. Zhou, R.A. Johnson, H.N.G. Wadley, Misfit-energy-increasing dislocations in vapor-deposited CoFe/NiFe multilayers, *Phys. Rev. B* 69 (2004) 144113, , <https://doi.org/10.1103/PhysRevB.69.144113>
- [77] D.-Y. Lin, S.S. Wang, D.L. Peng, M. Li, X.D. Hui, An *n*-body potential for a Zr-Nb system based on the embedded-atom method, *J. Phys. Condens. Matter* 25 (2013) 105404, , <https://doi.org/10.1088/0953-8984/25/10/105404>
- [78] A. Ghafarollahi, F. Maresca, W.A. Curtin, Solute/screw dislocation interaction energy parameter for strengthening in bcc dilute to high entropy alloys, *Model. Simul. Mater. Sci. Eng.* 27 (2019) 085011, , <https://doi.org/10.1088/1361-651X/ab4969>
- [79] R.A. Johnson, Alloy models with the embedded-atom method, *Phys. Rev. B* 39 (1989) 12554–12559, <https://doi.org/10.1103/PhysRevB.39.12554>
- [80] X.W. Zhou, H.N.G. Wadley, R.A. Johnson, D.J. Larson, N. Tabat, A. Cerezo, A.K. Petford-Long, G.D.W. Smith, P.H. Clifton, R.L. Martens, T.F. Kelly, Atomic scale structure of sputtered metal multilayers, *Acta Mater.* 49 (2001) 4005–4015, [https://doi.org/10.1016/S1359-6454\(01\)00287-7](https://doi.org/10.1016/S1359-6454(01)00287-7)
- [81] R.W. Smith, G.S. Was, Application of molecular dynamics to the study of hydrogen embrittlement in Ni-Cr-Fe alloys, *Phys. Rev. B* 40 (1989) 10322–10336, <https://doi.org/10.1103/PhysRevB.40.10322>
- [82] S. Xu, S.Z. Chavoshi, Y. Su, On calculations of basic structural parameters in multi-principal element alloys using small atomistic models, *Comput. Mater. Sci.* 202 (2022) 110942, , <https://doi.org/10.1016/j.commatsci.2021.110942>
- [83] A.P. Thompson, H.M. Aktulga, R. Berger, D.S. Bolintineanu, W.M. Brown, P.S. Crozier, P.J. in 't Veld, A. Kohlmeier, S.G. Moore, T.D. Nguyen, R. Shan, M.J. Stevens, J. Tranchida, C. Trott, S.J. Plimpton, LAMMPS - a flexible simulation tool for particle-based materials modeling at the atomic, meso, and continuum scales, *Comput. Phys. Commun.* 271 (2022) 108171, , <https://doi.org/10.1016/j.cpc.2021.108171>
- [84] P.M. Larsen, S. Schmidt, J. Schiott, Robust structural identification via polyhedral template matching, *Model. Simul. Mater. Sci. Eng.* 24 (2016) 055007, , <https://doi.org/10.1088/0965-0393/24/5/055007>
- [85] A. Stukowski, Visualization and analysis of atomistic simulation data with OVITO—the Open Visualization Tool, *Model. Simul. Mater. Sci. Eng.* 18 (2010) 015012, , <https://doi.org/10.1088/0965-0393/18/1/015012>
- [86] Y. Zhang, Y.J. Zhou, J.P. Lin, G.L. Chen, P.K. Liaw, Solid-solution phase formation rules for multi-component alloys, *Adv. Eng. Mater.* 10 (2008) 534–538, <https://doi.org/10.1002/adem.200700240>
- [87] G.J. Ackland, R. Thetford, An improved N-body semi-empirical model for body-centred cubic transition metals, *Philos. Mag. A* 56 (1987) 15–30, <https://doi.org/10.1080/01418618708204464>
- [88] F. Wang, G.H. Balbus, S. Xu, Y. Su, J. Shin, P.F. Rottmann, K.E. Knippling, J.-C. Stinville, L.H. Mills, O.N. Senkov, I.J. Beyerlein, T.M. Pollock, D.S. Gianola, Multiplicity of dislocation pathways in a refractory multiprincipal element alloy, *Science* 370 (2020) 95–101, <https://doi.org/10.1126/science.aba3722>
- [89] S. Xu, Y. Su, W.-R. Jian, I.J. Beyerlein, Local slip resistances in equal-molar MoNbTi multi-principal element alloy, *Acta Mater.* 202 (2021) 68–79, <https://doi.org/10.1016/j.actamat.2020.10.042>
- [90] R.A. Romero, S. Xu, W.-R. Jian, I.J. Beyerlein, C.V. Ramana, Atomistic simulations of the local slip resistances in four refractory multi-principal element alloys, *Int. J. Plast.* 149 (2022) 103157, , <https://doi.org/10.1016/j.ijplas.2021.103157>
- [91] S. Xu, W.-R. Jian, Y. Su, I.J. Beyerlein, Line-length-dependent dislocation glide in refractory multi-principal element alloys, *Appl. Phys. Lett.* 120 (2022) 061901, , <https://doi.org/10.1063/5.0008049>
- [92] E. Rabkin, D.J. Srolovitz, Onset of plasticity in gold nanopillar compression, *Nano Lett.* 7 (2007) 101–107, <https://doi.org/10.1021/nl0622350>
- [93] S. Xu, M.I. Latypov, Y. Su, Concurrent atomistic-continuum simulations of uniaxial compression of gold nano/submicropillars, *Philos. Mag. Lett.* 98 (2018) 173–182, <https://doi.org/10.1080/09500839.2018.1515506>
- [94] S. Xu, E. Hwang, W.-R. Jian, Y. Su, I.J. Beyerlein, Atomistic calculations of the generalized stacking fault energies in two refractory multi-principal element alloys, *Intermetallics* 124 (2020) 106844, , <https://doi.org/10.1016/j.intermet.2020.106844>
- [95] K. Cui, P.K. Liaw, Y. Zhang, Cryogenic-mechanical properties and applications of multiple-basis-element alloys, *Metals* 12 (2022) 2075, <https://doi.org/10.3390/met12122075>
- [96] S. Wang, M. Wu, D. Shu, G. Zhu, D. Wang, B. Sun, Mechanical instability and tensile properties of TiZrHfNbTa high entropy alloy at cryogenic temperatures, *Acta Mater.* 201 (2020) 517–527, <https://doi.org/10.1016/j.actamat.2020.10.044>
- [97] R.R. Eletti, N. Stepanov, S. Zherebtsov, Mechanical behavior and thermal activation analysis of HfNbTaTiZr body-centered cubic high-entropy alloy during tensile deformation at 77 K, *Scr. Mater.* 188 (2020) 118–123, <https://doi.org/10.1016/j.scriptamat.2020.07.028>